EUROPEAN ORGANISATION FOR NUCLEAR RESEARCH

CERN-PPE/94-108
15 July 1994

Measurements of the Inclusive Branching Ratios of τ-Leptons to K^0_S and Charged $K^*(892)$

The OPAL Collaboration

Abstract

We describe measurements of inclusive branching ratios of the tau lepton to K^0_S and charged $K^*(892)$ using $Z^0 \to \tau^+\tau^-$ candidates collected with the OPAL detector at LEP during 1990–1992. From a total of 61 854 tau candidates we find:

$$\begin{aligned} \mathrm{Br}(\tau^- \to K^0_S X^- \nu_\tau) &= 0.86 \pm 0.08(\mathrm{stat.}) \pm 0.05(\mathrm{syst.})\,\% \\ \mathrm{Br}(\tau^- \to K^{*-} \geq 0 h^0 \nu_\tau) &= 1.73 \pm 0.24(\mathrm{stat.}) \pm 0.13(\mathrm{syst.})\,\% \end{aligned}$$

where X^- refers to any configuration of particles with charge -1 and h^0 is any neutral hadron other than the K^0_S.

(to be submitted to Physics Letters B)

The OPAL Collaboration

R. Akers[16], G. Alexander[23], J. Allison[16], K.J. Anderson[9], S. Arcelli[2], S. Asai[24], A. Astbury[28], D. Axen[29], G. Azuelos[18,a], A.H. Ball[17], E. Barberio[26], R.J. Barlow[16], R. Bartoldus[3], J.R. Batley[5], G. Beaudoin[18], A. Beck[23], G.A. Beck[13], J. Becker[10], C. Beeston[16], T. Behnke[27], K.W. Bell[20], G. Bella[23], P. Bentkowski[18], S. Bentvelsen[8], P. Berlich[10], S. Bethke[32], O. Biebel[32], I.J. Bloodworth[1], P. Bock[11], H.M. Bosch[11], M. Boutemeur[18], S. Braibant[12], P. Bright-Thomas[25], R.M. Brown[20], A. Buijs[8], H.J. Burckhart[8], C. Burgard[27], P. Capiluppi[2], R.K. Carnegie[6], A.A. Carter[13], J.R. Carter[5], C.Y. Chang[17], C. Charlesworth[6], D.G. Charlton[8], S.L. Chu[4], P.E.L. Clarke[15], J.C. Clayton[1], S.G. Clowes[16], I. Cohen[23], J.E. Conboy[15], M. Coupland[14], M. Cuffiani[2], S. Dado[22], C. Dallapiccola[17], G.M. Dallavalle[2], C. Darling[31], S. De Jong[13], H. Deng[17], M. Dittmar[4], M.S. Dixit[7], E. do Couto e Silva[12], J.E. Duboscq[8], E. Duchovni[26], G. Duckeck[8], I.P. Duerdoth[16], U.C. Dunwoody[5], P.A. Elcombe[5], P.G. Estabrooks[6], E. Etzion[23], H.G. Evans[9], F. Fabbri[2], B. Fabbro[21], M. Fanti[2], M. Fierro[2], M. Fincke-Keeler[28], H.M. Fischer[3], P. Fischer[3], R. Folman[26], D.G. Fong[17], M. Foucher[17], J. Fowler[9], H. Fukui[24], A. Fürtjes[8], P. Gagnon[6], A. Gaidot[21], J.W. Gary[4], J. Gascon[18], N.I. Geddes[20], C. Geich-Gimbel[3], S.W. Gensler[9], F.X. Gentit[21], T. Geralis[20], G. Giacomelli[2], P. Giacomelli[4], R. Giacomelli[2], V. Gibson[5], W.R. Gibson[13], A. Giles[9], J.D. Gillies[20], J. Goldberg[22], D.M. Gingrich[30,a], M.J. Goodrick[5], W. Gorn[4], C. Grandi[2], P. Grannis[8], E. Gross[26], J. Hagemann[27], G.G. Hanson[12], M. Hansroul[8], C.K. Hargrove[7], J. Hart[8], P.A. Hart[9], M. Hauschild[8], C.M. Hawkes[8], E. Heflin[4], R.J. Hemingway[6], G. Herten[10], R.D. Heuer[8], J.C. Hill[5], S.J. Hillier[8], T. Hilse[10], D.A. Hinshaw[18], P.R. Hobson[25], D. Hochman[26], A. Höcker[3], R.J. Homer[1], A.K. Honma[28,a], R.E. Hughes-Jones[16], R. Humbert[10], P. Igo-Kemenes[11], H. Ihssen[11], D.C. Imrie[25], A. Jawahery[17], P.W. Jeffreys[20], H. Jeremie[18], M. Jimack[1], M. Jones[6], R.W.L. Jones[8], P. Jovanovic[1], C. Jui[4], D. Karlen[6], K. Kawagoe[24], T. Kawamoto[24], R.K. Keeler[28], R.G. Kellogg[17], B.W. Kennedy[20], B. King[8], J. King[13], S. Kluth[5], T. Kobayashi[24], M. Kobel[10], D.S. Koetke[8], T.P. Kokott[3], S. Komamiya[24], R. Kowalewski[8], R. Howard[29], P. Krieger[6], J. von Krogh[11], P. Kyberd[13], G.D. Lafferty[16], H. Lafoux[8], R. Lahmann[17], J. Lauber[8], J.G. Layter[4], P. Leblanc[18], P. Le Du[21], A.M. Lee[31], E. Lefebvre[18], M.H. Lehto[15], D. Lellouch[26], C. Leroy[18], J. Letts[4], L. Levinson[26], Z. Li[12], F. Liu[29], S.L. Lloyd[13], F.K. Loebinger[16], G.D. Long[17], B. Lorazo[18], M.J. Losty[7], X.C. Lou[8], J. Ludwig[10], A. Luig[10], M. Mannelli[8], S. Marcellini[2], C. Markus[3], A.J. Martin[13], J.P. Martin[18], T. Mashimo[24], P. Mättig[3], U. Maur[3], J. McKenna[29], T.J. McMahon[1], A.I. McNab[13], J.R. McNutt[25], F. Meijers[8], F.S. Merritt[9], H. Mes[7], A. Michelini[8], R.P. Middleton[20], G. Mikenberg[26], J. Mildenberger[6], D.J. Miller[15], R. Mir[26], W. Mohr[10], C. Moisan[18], A. Montanari[2], T. Mori[24], M. Morii[24], U. Müller[3], B. Nellen[3], B. Nijjhar[16], S.W. O'Neale[1], F.G. Oakham[7], F. Odorici[2], H.O. Ogren[12], C.J. Oram[28,a], M.J. Oreglia[9], S. Orito[24], J.P. Pansart[21], G.N. Patrick[20], M.J. Pearce[1], P. Pfister[10], P.D. Phillips[16], J.E. Pilcher[9], J. Pinfold[30], D. Pitman[28], D.E. Plane[8], P. Poffenberger[28], B. Poli[2], A. Posthaus[3], T.W. Pritchard[13], H. Przysiezniak[18], M.W. Redmond[8], D.L. Rees[8], D. Rigby[1], M. Rison[5], S.A. Robins[13], D. Robinson[5], J.M. Roney[28], E. Ros[8], S. Rossberg[10], A.M. Rossi[2], M. Rosvick[28], P. Routenburg[30], Y. Rozen[8], K. Runge[10], O. Runolfsson[8], D.R. Rust[12], M. Sasaki[24], C. Sbarra[2], A.D. Schaile[8], O. Schaile[10], F. Scharf[3], P. Scharff-Hansen[8], P. Schenk[4], B. Schmitt[3], H. von der Schmitt[11], M. Schröder[12], H.C. Schultz-Coulon[10], P. Schütz[3], M. Schulz[8], C. Schwick[27], J. Schwiening[3], W.G. Scott[20], M. Settles[12], T.G. Shears[5], B.C. Shen[4], C.H. Shepherd-Themistocleous[7], P. Sherwood[15], G.P. Siroli[2], A. Skillman[16], A. Skuja[17], A.M. Smith[8], T.J. Smith[28], G.A. Snow[17], R. Sobie[28], R.W. Springer[17], M. Sproston[20], A. Stahl[3], C. Stegmann[10], K. Stephens[16], J. Steuerer[28], B. Stockhausen[3], R. Ströhmer[11], D. Strom[19], P. Szymanski[20], H. Takeda[24], T. Takeshita[24], S. Tarem[26], M. Tecchio[9], P. Teixeira-Dias[11], N. Tesch[3], M.A. Thomson[15], S. Towers[6], T. Tsukamoto[24], M.F. Turner-Watson[8], D. Van den plas[18], R. Van Kooten[12], G. Vasseur[21], M. Vincter[28], A. Wagner[27], D.L. Wagner[9], C.P. Ward[5], D.R. Ward[5], J.J. Ward[15], P.M. Watkins[1], A.T. Watson[1], N.K. Watson[7], P. Weber[6], P.S. Wells[8], N. Wermes[3],

B. Wilkens[10], G.W. Wilson[4], J.A. Wilson[1], V-H. Winterer[10], T. Wlodek[26], G. Wolf[26], S. Wotton[11], T.R. Wyatt[16], A. Yeaman[13], G. Yekutieli[26], M. Yurko[18], W. Zeuner[8], G.T. Zorn[17].

[1]School of Physics and Space Research, University of Birmingham, Birmingham B15 2TT, UK
[2]Dipartimento di Fisica dell' Università di Bologna and INFN, I-40126 Bologna, Italy
[3]Physikalisches Institut, Universität Bonn, D-53115 Bonn, Germany
[4]Department of Physics, University of California, Riverside CA 92521, USA
[5]Cavendish Laboratory, Cambridge CB3 0HE, UK
[6]Carleton University, Department of Physics, Colonel By Drive, Ottawa, Ontario K1S 5B6, Canada
[7]Centre for Research in Particle Physics, Carleton University, Ottawa, Ontario K1S 5B6, Canada
[8]CERN, European Organisation for Particle Physics, CH-1211 Geneva 23, Switzerland
[9]Enrico Fermi Institute and Department of Physics, University of Chicago, Chicago IL 60637, USA
[10]Fakultät für Physik, Albert Ludwigs Universität, D-79104 Freiburg, Germany
[11]Physikalisches Institut, Universität Heidelberg, D-69120 Heidelberg, Germany
[12]Indiana University, Department of Physics, Swain Hall West 117, Bloomington IN 47405, USA
[13]Queen Mary and Westfield College, University of London, London E1 4NS, UK
[14]Birkbeck College, London WC1E 7HV, UK
[15]University College London, London WC1E 6BT, UK
[16]Department of Physics, Schuster Laboratory, The University, Manchester M13 9PL, UK
[17]Department of Physics, University of Maryland, College Park, MD 20742, USA
[18]Laboratoire de Physique Nucléaire, Université de Montréal, Montréal, Quebec H3C 3J7, Canada
[19]University of Oregon, Department of Physics, Eugene OR 97403, USA
[20]Rutherford Appleton Laboratory, Chilton, Didcot, Oxfordshire OX11 0QX, UK
[21]CEA, DAPNIA/SPP, CE-Saclay, F-91191 Gif-sur-Yvette, France
[22]Department of Physics, Technion-Israel Institute of Technology, Haifa 32000, Israel
[23]Department of Physics and Astronomy, Tel Aviv University, Tel Aviv 69978, Israel
[24]International Centre for Elementary Particle Physics and Department of Physics, University of Tokyo, Tokyo 113, and Kobe University, Kobe 657, Japan
[25]Brunel University, Uxbridge, Middlesex UB8 3PH, UK
[26]Particle Physics Department, Weizmann Institute of Science, Rehovot 76100, Israel
[27]Universität Hamburg/DESY, II Institut für Experimental Physik, Notkestrasse 85, D-22607 Hamburg, Germany
[28]University of Victoria, Department of Physics, P O Box 3055, Victoria BC V8W 3P6, Canada
[29]University of British Columbia, Department of Physics, Vancouver BC V6T 1Z1, Canada
[30]University of Alberta, Department of Physics, Edmonton AB T6G 2J1, Canada
[31]Duke University, Dept of Physics, Durham, NC 27708-0305, USA
[32]Technische Hochschule Aachen, III Physikalisches Institut, Sommerfeldstrasse 26-28, D-52056 Aachen, Germany

[a]Also at TRIUMF, Vancouver, Canada V6T 2A3

1 Introduction

Measurements of the inclusive branching ratios of τ^- leptons to K^0_S, and to $K^{*-}(892)$ accompanied by ≥ 0 neutral hadrons[1], are presented in this paper. These measurements were made using data collected with the OPAL detector at LEP during the 1990–1992 running periods The dominant source of K^0_S in tau decays is expected to be the $K^{*-}(892)$ resonance from the exclusive decay $\tau^- \to K^{*-}\nu_\tau$. The branching ratio of this Cabibbo-suppressed decay can be predicted from the $\tau^- \to \rho^- \nu_\tau$ branching ratio using asymptotic flavor symmetry[1, 2], which relates the strange and non-strange hadronic current coupling strengths to the W boson (g_{K^*}, g_ρ) to the masses (M_{K^*}, M_ρ): $g_{K^*}/g_\rho = M_{K^*}/M_\rho$. The measured $\tau^- \to \rho^- \nu_\tau$ branching ratio of 24.0±0.6% [3], taken together with the above relationship and the value of the Cabibbo angle ($\tan\theta_c$=0.23 [3]), then implies that $Br(\tau^- \to K^{*-}\nu_\tau) \sim 1.2\%$, in reasonable agreement with the current average measured value of 1.42±0.18% [3].

At OPAL, K^0_S mesons are identified by their decay to $\pi^+\pi^-$. The decay chain of interest is

$$\begin{array}{lllll} \tau^- \to & K^{*-}\nu_\tau & & & (B.R. = 1.4\%) \\ & \hookrightarrow & K^0_S\pi^- & & (B.R. = 33\%) \\ & & \hookrightarrow & \pi^+\pi^- & (B.R. = 68.6\%) \end{array} \qquad (1)$$

with a product branching ratio of approximately 0.3%.

The decay $\tau^- \to K^{*-}\nu_\tau$, although expected to be dominant, is not necessarily the only source of K^0_S in tau decays. K^0_S mesons may also come from decays of higher mass resonances such as the $\rho(1700)$, the $K^*(1410)$, or the K_1 resonances, or may be produced in non-resonant decays. Theoretical predictions for the summed branching ratio of tau decay channels to K^0_S, other than the dominant $\tau^- \to K^{*-}\nu_\tau$, are generally <0.4% [4, 5]. These decays, however, are especially interesting as high mass resonances are useful in setting bounds on the tau-neutrino mass [6], and since tau decays to K_1 can be used to measure the strength of effective second class currents in strange charged current couplings [7].

Experimentally, K^0_S, exclusive K^* ($\tau^- \to K^{*-}\nu_\tau$), inclusive K^* ($\tau^- \to K^{*-} \geq 0h^0\nu_\tau$), and multi-kaon production in tau decays have been measured by several groups at e^+e^- colliders [8–15].

2 Event Selection

The OPAL Detector

As the analysis presented in this letter depends heavily upon tracking, a brief description of the OPAL central tracking system is given below. The OPAL detector as a whole is described in detail elsewhere [16].

The central tracking chambers at OPAL are contained in a 4 bar pressure vessel and immersed in a 0.435 T axial magnetic field. Moving from small to large radius, the tracking system consists of a 1 m long precision vertex drift chamber with 12 axial wires and 6 small angle (4°) stereo wires extending in radius from ∼10–21 cm, a large volume (4 m long, 3.7 m diameter) drift chamber (jet-chamber) with 159 layers of axial anode wires, and z-chambers which provide up to six precise measurements of the z-coordinate[2] of charged particles as they leave the tracking system. Before the 1991 run a silicon micro-vertex detector was also installed with silicon planes at radii of 6.1 and 7.5

[1] Charge conjugation is implied throughout this paper. Also, the symbol K^* will be used to indicate the $K^{*-}(892)$ particle and neutral hadrons denoted h^0 will be taken to exclude K^0_S.

[2] In the OPAL coordinate system the z-axis follows the electron beam, the x-axis lies horizontally in the plane of LEP, and the y-axis is perpendicular to the plane. The polar angle θ is defined relative to the $+z$-axis, while the azimuthal angle ϕ is measured relative to the $+x$-axis.

cm [17]. The jet-chamber allows the full 159 measurements over the polar angle range $|\cos\theta| < 0.73$, while the z-chambers provide measurements to $|\cos\theta| < 0.72$. The momentum in the r-ϕ plane, p_t, is measured in the region $|\cos\theta| < 0.73$ with a resolution of $(\sigma(p_t)/p_t)^2 \sim 0.02^2 + (0.0015 \cdot p_t)^2$ (p_t in GeV). The jet-chamber also provides measurements of the energy loss (dE/dx) of tracks. The dE/dx resolution achieved in multi-hadronic events is ~3.5% for tracks with the maximum number of space point samples.

Selection of $e^+e^- \to \tau^+\tau^-$ Events

The procedure used to select tau pair events, and to estimate the residual backgrounds after the selection, has been described in detail elsewhere[18]. Events were accepted if they fell within $|\cos\theta_{\rm ave}|<0.72$, where $\theta_{\rm ave}$ is the average θ of the two tau jets defined using tracks and clusters in the electromagnetic calorimeter (which is composed of lead-galss blocks approximately 25 radiation lengths in depth): 30 927 events (61 854 taus) passed this selection in the 1990-1992 data sets. The numbers of tau candidates per year are shown in table 1.

The efficiency of the $e^+e^- \to \tau^+\tau^-$ selection (called the *pre-selection* in the following) was estimated from Monte Carlo simulation[5, 19] to be ~59%. This corresponds to an efficiency within the angular acceptance of ~92%. Background contamination in the pre-selection from $e^+e^- \to e^+e^-$, $e^+e^- \to \mu^+\mu^-$, $e^+e^- \to q\bar{q}$, and $e^+e^- \to (e^+e^-)X$ was also estimated using Monte Carlo calculations. Corrections were then applied to the Monte Carlo background predictions using control samples of electrons, muons, and hadrons from the data. The total background fraction was found to be $f^{\rm non-\tau}_{\rm pre-sel} = 1.76 \pm 0.44\%$. The bias, with respect to the average acceptance of the pre-selection cuts for all tau decay modes, for the $\tau \to K^* \to K^0_S$ sample was estimated using Monte Carlo generated $\tau^- \to K^{*-}\nu_\tau$ events where the K^{*-} was forced to decay to K^0_S. The bias factor, which is defined as the ratio of the efficiency of the pre-selection for finding $\tau \to K^* \to K^0_S$ events to the average pre-selection efficiency for all tau decay modes, was found to be $f^{\rm bias}(\tau \to K^* \to K^0_S) = 1.016 \pm 0.012$.

The pre-selection background fractions, and the bias factors are listed in table 2 for each year. As the detector configuration did not change between the 1991 and 1992 runs, efficiencies, backgrounds, and biases are expected to be the same for those two data sets. The absence of the silicon micro-vertex detector in the 1990 run could have caused differences in the values between 1991 and 1990. As can be seen, however, no significant differences are observed, and therefore averages of the values over the three years were used in the analysis and all of the data were treated simultaneously.

Secondary Vertex Finding

$K^0_S \to \pi^+\pi^-$ candidates were identified by looking for intersections of oppositely charged tracks in the x-y plane. Only good quality tracks having at least 20 jet-chamber hits, a track-fit χ^2 per degree of freedom in the x-y plane of less than 8, a momentum transverse to the beam direction, p_t, of at least 50 MeV, and a measured momentum of not more than 100 GeV were used. Background from tracks originating at the primary vertex was suppressed by requiring the sum of the radial distances of each track from the primary vertex at the point of closest approach in the x-y plane ($\sum |d_0|$) to be at least 2 mm.

To be considered as good secondary vertices, track pair intersections had to occur outside a region centered around the beamspot, defined as a cylinder of radius 1 cm and length 10 cm, and inside a radial distance from the primary vertex of 150 cm. The tracks of the pair also had to be separated in z at the intersection point by less than 20 cm. Because tracks describe circles in the x-y plane, two intersections occur for each track pair. Intersections occuring at radii greater than the true vertex were, in general, rejected by requiring that no hits associated with either track occurred at a distance of greater than 6 cm inside the radius of the secondary vertex.

	1990	1991	1992	Total
Pre-Selected taus ($N_\tau^{pre-sel}$)	6 476	16 110	39 268	61 854
Identified Conversions (rejected)	288	827	2 047	3 162
Vertex Candidates (conversions removed)	504	1 489	3 585	5 578
Inclusive K^0_S ($N(\text{incl-}K^0_S)$)	17	37	87	141
$K^0_S h^- \geq 0h^0$ ($N(K^0_S h^- \geq 0h^0)$)	16	28	76	120

Table 1: The numbers of candidates selected (or rejected in the case of conversions) by the various stages of the analysis in each year of the data.

	1990	1991-1992	Total / Average
Backgrounds (%):			
$e^+e^- \to e^+e^-$	0.20±0.20	0.22±0.08	0.22±0.07
$e^+e^- \to \mu^+\mu^-$	0.80±0.90	0.91±0.46	0.89±0.41
$e^+e^- \to q\bar{q}$	0.70±0.30	0.42±0.18	0.49±0.15
$e^+e^- \to (e^+e^-)X$	0.20±0.20	0.16±0.03	0.16±0.03
Total			1.76±0.44
$f^{bias}(\tau \to K^* \to K^0_S)$	1.010±0.028	1.017±0.014	1.016±0.012

Table 2: The estimated background fractions, and $\tau \to K^* \to K^0_S$ bias factor for the $e^+e^- \to \tau^+\tau^-$ pre-selection.

In order to the estimate the secondary vertex fit quality, a quantity X is defined as

$$X = \left(\frac{\Delta z}{5\text{cm}}\right)^2 + \left(\frac{\sin\alpha}{0.015}\right)^2 \tag{2}$$

where Δz is the separation in z of the two tracks at the intersection and α is the angle between the momentum vector of the neutral particle which decays to form the vertex and its flight path (a vector from the primary vertex to the secondary vertex position). High quality vertex fits were selected by demanding $X \leq 25$.

After a good intersection was found, the two tracks were re-fit with the constraint that they both originated from the secondary vertex in z. The vertex was rejected if the χ^2 of either of these re-fitted tracks was greater than 100. If both intersections of a track pair satisfied the above cuts, the intersection with the lowest value of X was chosen.

The vertex finder also identifies photon conversion candidates. Conversion candidates were found (and rejected from this analysis) by an algorithm which searches for oppositely charged tracks which have parallel tangents at a point where they pass close to each other and dE/dx values consistent with an electron hypothesis.

The numbers of secondary vertex candidates (V_0) and rejected conversions per year are shown in table 1.

Multi-Hadronic Event Rejection

Contamination of the final event samples with multi-hadronic (MH) events from $e^+e^- \to q\bar{q}$ is an especially serious background as a large fraction of these MH events contain at least one K^0_S. In order to reduce this background cuts were made on the invariant mass of all good tracks (as defined in the $K^0_S h^- \geq 0 h^0$ selection below) in both the hemispheres containing, and opposite to, the K^0_S momentum vector:

- $M_{\rm hemi} < 2.0$ GeV (for each hemisphere).

These cuts reject almost all MH events while retaining nearly 99% of the $\tau \to K^0_S$ signal. Residual contamination of the final data samples with MH events is discussed later as a systematic error.

Final Selections

After secondary vertices were identified, a set of tighter cuts were applied to the events to reduce remaining backgrounds, which were mainly due to false vertices from random crossings of oppositely charged tracks. Two selections were made to identify inclusive K^0_S and inclusive $K^0_S h^- \geq 0 h^0$ production in tau decays. Briefly, the K^0_S selection required a good K^0_S candidate in the event with no other requirements on the number of tracks and neutral clusters in the same hemisphere as the K^0_S (above those already applied by the pre-selection). The $K^0_S h^- \geq 0 h^0$ selection demanded a good K^0_S plus any number of neutral particles, but only one other good charged track in the same hemisphere as the K^0_S.

Inclusive K^0_S Selection

The following track quality cuts were applied to both of the tracks in the vertex:

- number of z-chamber hits > 3
- $0.15 < p_t < 25.0$ GeV

Good quality vertices were selected by requiring:

- the angle between the momentum vector and flight-path of the V_0: $\alpha < 4$ mrad
- the invariant mass calculated assuming the tracks to be electrons: $M_V(e^+e^-) > 150$ MeV (applied to reduce remaining contamination from conversions)
- the invariant mass calculated assuming the tracks to be pions close to $M_{K^0_S}$: $475 < M_V(\pi^+\pi^-) < 520$ MeV.

The final cut on $M_V(\pi^+\pi^-)$ corresponds to a window of approximately $\pm 3\sigma$ in the detector's invariant mass resolution for $K^0_S \to \pi^+\pi^-$ decays in the momentum range being considered here.

A total of 141 events were selected with these cuts in the 1990–1992 data samples. A year-by-year breakdown is given in table 1. Distributions of several of the variables used in the analysis are shown in figure 1. The V_0 invariant mass distribution (assuming the tracks to be pions) is shown in figure 2. In figure 1, distributions from background events not coming from K^0_S were estimated from data events with $M_V(\pi^+\pi^-)$ outside of the K^0_S mass window and are shown as cross-hatched histograms. Agreement between the data and the sum of background plus Monte Carlo generated signal events is, in general, quite good for all distributions. Some discrepancy, however, is observed at low values of α (figure 1 b). This occurs far from the cut value of 4 mrad and is discussed later as a systematic error.

$K^0_S h^- \geq 0 h^0$ Selection

By pairing the K^0_S candidates selected as above with a charged track in the same hemisphere, K^* candidates could be defined. The following requirements were placed on tracks associated with K^0_S's to define the $K^0_S h^- \geq 0 h^0$ selection:

- track momentum vector in the same hemisphere as the K^0_S momentum vector
- number of jet-chamber hits > 80
- number of z-chamber hits > 3
- $p_t > 0.15$ GeV
- the point of closest approach of the track to the primary vertex in the x-y plane: $|d_0| < 0.5$ cm
- the point of closest approach of the track to the primary vertex in z: $|z_0| < 5.0$ cm
- the radius of the first hit in the jet chamber < 75 cm.

The event was accepted if **exactly one** track satisfied these requirements.

The last three cuts listed ensured that the track paired with the K^0_S originated near the primary vertex, and thus decreased backgrounds due to conversions and nuclear interactions. The number of tracks fulfilling these requirements per K^0_S candidate is shown in figure 1 d).

Finally, the invariant mass of the K^0_S-h^- system was calculated assuming the h^- was a π^-. In the calculation the oppositely charged tracks forming the V_0 were constrained such that their invariant mass was equal to $M_{K^0_S}$. The K^0_S-h^- invariant mass distribution is given in figure 3. Only events in the K^0_S-h^- invariant mass region 0.625–1.350 GeV were considered in the branching ratio calculation. In total, 120 data events passed the $K^0_S h^- \geq 0 h^0$ cuts. Year-by-year statistics are again given in table 1.

3 Signal and Background Estimation

The background under the K^0_S mass peak, from misidentified vertices due to random crossings of oppositely charged tracks, was estimated by sideband subtraction. The average of the number of events per 5 MeV bin in $M_V(\pi^+\pi^-)$ from a high and a low sideband region (0.40–0.45 GeV and 0.55–0.60 GeV respectively), assumed to contain only background events, was used to estimate the background in the signal region (0.475–0.520 GeV). The $M_V(\pi^+\pi^-)$ distribution for those events in the inclusive K^0_S sample, without the $M_V(\pi^+\pi^-)$ cut, including the signal and sideband regions is shown in figure 2. The background predicted in the signal region from misidentified vertices, using the sideband subtraction technique, was found to be 13.1 ± 2.4 out of the total of 141 events.

The fraction of $\tau^- \to K^{*-} \geq 0 h^0 \nu_\tau$ events in the $K^0_S h^- \geq 0 h^0$ data sample was found by a binned log-likelihood fit of a spin-1 Breit-Wigner resonance K^{*-} signal plus a non-K^{*-} shape parameterized by a second order polynomial. The peak of the Breit-Wigner was fixed at the nominal value of 892 MeV, and the width, Γ, was taken to be 75 MeV, corresponding to the width observed in Monte Carlo $\tau^- \to K^{*-} \nu_\tau$ events which is a convolution of the natural K^* width (49.8 ± 0.8 MeV [3]) with detector effects. The fit was performed over the mass region 0.625–1.350 GeV. Parameters allowed to vary in the fit were the fraction of the Breit-Wigner signal in the sample (f_{K^*}) and the three coefficients of the second order polynomial. Results of the fit to the data are shown in figure 3 and indicate that $61.9 \pm 6.4\%$ of the $K^0_S h^- \geq 0 h^0$ events contain a real K^{*-}.

It is evident from both the shape of the K^0_S-h^- invariant mass spectrum and from the fitted fraction of K^* events that a substantial non-K^* component exists in the $\tau^- \to K^0_S h^- \geq 0 h^0 \nu_\tau$ data.

This non-K^* component could be composed of two types of events – those where an incorrectly identified vertex fakes a K^0_S (the non-K^0_S events), and those where a real K^0_S is present but was not the product of a K^{*-} decay (the non-K^* events). The non-K^0_S background was estimated using the same sideband subtraction technique as for the K^0_S background described above, on the $\pi^+\pi^-$ mass spectrum of those events in the $K^0_S h^- \geq 0h^0$ sample with the $M_V(\pi^+\pi^-)$ cut relaxed. The fitted background under the K^0_S peak in this sample indicates that 8.1 ± 1.9 of the 120 $K^0_S h^- \geq 0h^0$ candidates do not contain K^0_S mesons. Thus, 31% of the events in the inclusive K^* sample arise from the decay $\tau^- \to K^0_S h^- \geq 0h^0 \nu_\tau$ but do not go through the K^{*-} resonance.

4 Selection Efficiency Calculation

The efficiency of the cuts to select inclusive K^0_S and K^* events from the $e^+e^- \to \tau^+\tau^-$ pre-selection was calculated using Monte Carlo data samples generated with KORALZ 4.0 [19] including initial and final state radiation for $e^+e^- \to \tau^+\tau^-$, and TAUOLA 2.5 [5] for the subsequent tau decays. These Monte Carlo events were then passed through a detailed simulation of the OPAL detector [20] and were subjected to the same analysis chain as the data.

The efficiency of the inclusive K^0_S cuts, as a function of the K^0_S $\cos\theta$ and momentum, is presented in figures 4 a) and b). This efficiency is calculated *with respect to the* $e^+e^- \to \tau^+\tau^-$ *pre-selection* using Monte Carlo $\tau \to K^* \to K^0_S$ events with $K^0_S \to \pi^+\pi^-$. Although no significant efficiency dependence on θ is observed, the efficiency (mainly of the vertex finder) falls with increasing momentum. The Monte Carlo, however, reproduces the K^0_S and K^* momentum spectra fairly well, as can be seen in figures 4 c) and d). Because of this, global efficiencies were used in the branching ratio calculation

$$\begin{aligned} \varepsilon(\text{incl-}K^0_S) &= 24.1\pm0.4\% \\ \varepsilon(K^0_S h^- \geq 0h^0) &= 6.9\pm0.1\%. \end{aligned} \tag{3}$$

Note that these efficiencies include the $K^0_S \to \pi^+\pi^-$ branching ratio of $68.61\pm0.28\%$ [3], and the $K^{*-} \to K^0_S \pi^-$ branching ratio of 1/3 from isospin arguments is included in $\varepsilon(K^0_S h^- \geq 0h^0)$. The errors are due to the statistics of the Monte Carlo event sample.

5 Branching Ratio Calculations

Branching ratios were calculated from the number of pre-selected $e^+e^- \to \tau^+\tau^-$ events using the following formulas.

$$\begin{aligned} \text{Br}(\tau^- \to K^0_S X^- \nu_\tau) &= \frac{[N(\text{incl-}K^0_S) - N^{\text{bgrd}}(\text{incl-}K^0_S)]}{N_\tau^{\text{pre-sel}}(1 - f^{\text{non-}\tau}_{\text{pre-sel}})} \frac{1}{\varepsilon(\text{incl-}K^0_S)} \frac{1}{f^{\text{bias}}(\tau \to K^* \to K^0_S)} \\ &= 0.86 \pm 0.08\% \end{aligned} \tag{4}$$

$$\begin{aligned} \text{Br}(\tau^- \to K^{*-} \geq 0h^0 \nu_\tau) &= \frac{f_{K^*} N(K^0_S h^- \geq 0h^0)}{N_\tau^{\text{pre-sel}}(1 - f^{\text{non-}\tau}_{\text{pre-sel}})} \frac{1}{\varepsilon(K^0_S h^- \geq 0h^0)} \frac{1}{f^{\text{bias}}(\tau \to K^* \to K^0_S)} \\ &= 1.73 \pm 0.24\% \end{aligned} \tag{5}$$

where $N^{\text{bgrd}}(\text{incl-}K^0_S)$ is the fitted background under the signal $M_V(\pi^+\pi^-)$ mass region. The errors quoted on the above numbers are the statistical errors from the fit resulting from the number of signal and background events.

Source	σ/Br (%)	
	$\tau^- \to K^0_S X^- \nu_\tau$	$\tau^- \to K^{*-} \geq 0 h^0 \nu_\tau$
Signal Estimation Method:		
Gauss+Linear	2.3	—
K^* Sideband Subtr.	—	4.7
$M_V(\pi^+\pi^-)$ mass-window	0.8	0.8
$M_V(\pi^+\pi^-)$ sidebands	0.7	—
MH Rejection	2.8	3.9
Vertex Finder Efficiency	3.0	3.0
MC Statistics: Efficiency	1.7	1.9
f^{bias}	1.2	1.2
Track p_t-Spectrum	1.3	1.3
Z-Chamber Hits	0.3	0.3
α	0.2	0.2
Residual Conversions (M_{ee})	1.5	1.5
$f^{non-\tau}_{pre-sel}$	0.5	0.5
Total	**5.6**	**7.5**
Statistical	**9.5**	**13.9**

Table 3: Relative systematic errors on the branching ratio measurements.

6 Cross Checks and Systematic Errors

Several cross checks on the reliability of the assumptions used in the branching ratio calculation have been performed. Various sources of systematic error have also been identified. Descriptions of the cross checks and of the methods used to obtain the systematic errors are explained in more detail below. Estimates of the sizes of the systematic effects are summarized in table 3.

Signal Estimation Methods

In order to estimate the size of biases arising from the assumptions made in estimating the signal and background in the inclusive K^0_S sample, the background was estimated using a fit to the $M_V(\pi^+\pi^-)$ distribution of the K^0_S candidates without the $M_V(\pi^+\pi^-)$ cut. The fit function used was the sum of a Gaussian plus a linear background, and was fit to the $M_V(\pi^+\pi^-)$ spectrum over the mass range 0.4–0.6 GeV. All 5 parameters of this function – the amplitude, mean, and width of the Gaussian, and the constant and slope terms of the background – were allowed to vary in the fit, the results of which are shown in figure 2. As can be seen from figure 2 the fitted mean mass in the data (497.8$\pm$0.5 MeV) agrees well with that predicted from Monte Carlo $\tau \to K^* \to K^0_S$ events (497.7$\pm$0.1 MeV), and both are consistent with the world average value, 497.671$\pm$0.031 MeV[3]. The width of the K^0_S peak ($\sim$7 MeV) is also consistent in data and Monte Carlo.

Integrating the fitted background over the signal region (0.475–0.520 GeV) leads to an estimate of 16.0$\pm$2.5 background events in the 141 K^0_S candidates, which is consistent with the background predicted by the sideband subtraction method (13.1$\pm$2.4). The difference between these two estimates was used as the systematic error from the background estimation method.

Effects on the measured branching ratio because of leakage of signal events out of the $\pi^+\pi^-$ mass window used to define K^0_S candidates and from the definition of the sideband regions used to estimate the background were studied by repeating the analysis using several different mass windows to calculate the signal and efficiency and using several different sideband regions to estimate the background. Signal mass windows were varied by up to $\pm$10 MeV, and sidebands encompassing the entire regions 0.350–0.475 and 0.550–0.800 GeV were used. The average differences from the standard branching ratio were used as estimates of the systematic errors from these two effects.

In the inclusive K^* sample the systematic error due to assumptions made in the fit function used to extract f_{K^*} was estimated by calculating the number of K^{*-} events in the K^0_S-h^- invariant mass distribution using a sideband subtraction technique. The signal region for this sideband subtraction was defined as 0.75–1.10 GeV and the low and high sidebands (assumed to contain only non-K^{*-} events) were taken to be 0.65–0.75 GeV and 1.10–1.30 GeV respectively. The difference in the $\tau^-\to K^{*-}\geq 0h^0\nu_\tau$ branching ratio calculated using the standard fit and the sideband subtraction was used as the systematic error from the signal extraction method in this sample.

The validity of the Breit-Wigner parameters used in the fit function was checked using a fit to the data allowing the Breit-Wigner peak and width to vary, as well as f_{K^*} and the second order polynomial parameters. The results of this fit agree statistically with the standard fit, and give a fitted mass and width of 889$\pm$6 MeV and 95$\pm$16 MeV, respectively. These values also agree with the K^{*-} parameters measured by the OPAL collaboration in hadronic Z^0 decays [21] although the width seen in this analysis is larger because of the harder K^* momentum spectrum in tau decays. No additional systematic covering uncertainties in the Breit-Wigner parameters was therefore assigned.

The consistency of the assumption on the shape of the non-K^{*-} component was checked by using different parameterizations of the shape of the non-K^{*-} $M(K^0_S$-$h^-)$ spectrum in the fit, including a parameterization of the $M(K^0_S$-$h^-)$ spectrum from Monte Carlo $\tau^-\to K^0_S\pi^-\pi^0$ events. Results obtained from these checks were again consistent with those of the standard fit, and thus no systematic error was assigned due to the non-K^{*-} parameterization.

Background from $e^+e^-\to q\bar{q}$

Most multi-hadronic (MH) background in the final event samples was removed by the $M_{\rm hemi}$ cuts. A systematic error, however, is assigned to take into account the possibility of some residual MH contamination in the final samples. The unweighted average of two independent estimates of the number of $e^+e^-\to q\bar{q}$ events remaining after the cuts (see table 4) was used as a measure of the systematic uncertainty from the $e^+e^-\to q\bar{q}$ rejection.

First, low multiplicity Monte Carlo MH events were put through the analysis chain. No events passed the inclusive K^0_S cuts. Low multiplicity MH events, however, may not be well modelled in the Monte Carlo. For this reason data events were also used to check the $e^+e^-\to q\bar{q}$ contamination.

Decays in the opposite hemisphere from the K^0_S in the inclusive K^0_S and K^* samples should be normal tau decays with the standard ratio of 1:3:5 prong decays. Deviations from the standard ratios were measured by counting the number of events with more than 1 well measured charged track in the opposite hemisphere from the K^0_S. All events with one charged track in the opposite hemisphere were assumed to come from tau decays. The excess of multi-prong events in the data from what would be expected by applying the measured[3] 3- and 5- to 1-prong ratio to the number of 1-prong data events, was taken to be a measure of the residual MH contamination in the samples.

As can be seen from table 4, the predictions of residual MH contamination in the data samples are either equal to or consistent with zero. Because of this, no correction was applied, but the unweighted average of the two predictions was used as the systematic error.

Vertex Finder Efficiency

Uncertainty in the modelling of the efficiency for finding secondary vertices, which is estimated

Sample	$\tau^- \to K^0_S X^- \nu_\tau$	$\tau^- \to K^{*-} \geq 0 h^0 \nu_\tau$
MH MC	0±4.2	0±4.2
1- vs >1-Prong	7.2±5.5	5.9±5.1
Average	3.6	2.9

Table 4: Predicted numbers of multi-hadronic events in the inclusive K^0_S and K^* data samples. The errors on the MH MC predictions are 90% confidence level limits.

to be ∼58% for Monte Carlo $\tau \to K^0_S \to \pi^+\pi^-$ events, introduces a systematic error on the branching ratio measurements. The main loss in efficiency of the vertex finder comes from the $\sum |d_0|$ cut ($\sum |d_0| > 2$ mm), which also dominates the systematic error from the vertex finder efficiency. This systematic error was estimated using $\Lambda \to p\pi^-$ and $K^0_S \to \pi^+\pi^-$ decays in MH events [22]. By using MH events, a significant increase in the statistics of the secondary vertex sample could be gained over the $\tau \to K^0_S$ data sample, allowing a more precise estimate of possible systematic effects. The size of these systematic effects was estimated by comparing the agreement between data and Monte Carlo when varying the $|d_0|$, α, and number of jet-chamber hits cuts. The main discrepancy was found when varying the $|d_0|$ cut, which is the dominant contribution to the systematic error of 3% from these studies.

It should be noted that the systematic error estimated above using multi-hadronic events should be an upper limit on the size of possible effects in the $\tau \to K^0_S$ data because of the more complicated tracking environment in the multi-hadronic events. Nevertheless, several checks have been performed on vertex finding in the tau environment and are summarized below.

Shown in figure 5 is the $\sum |d_0|$ distribution for those events in the inclusive K^0_S sample where the $\sum |d_0|$ cut has not been applied in the vertex finder. In the figure, data are compared with the sum of the MC prediction for the $\tau \to K^0_S \to \pi^+\pi^-$ signal plus an estimate of the $\sum |d_0|$ distribution of misidentified vertices obtained from events passing all the inclusive K^0_S cuts but lying outside the $M_V(\pi^+\pi^-)$ signal region (0.475–0.520 GeV). A total of 141 data events pass the cut $\sum |d_0| > 2$ mm, while 148.9 events are predicted from the MC signal plus misidentified vertex background distribution. These two numbers are statistically consistent, giving confidence that the $\sum |d_0|$ distribution is well understood. No further systematic error, beyond that from the multi-hadronic studies, was assigned because of uncertainties in the modelling of $\sum |d_0|$.

In order to check the effect of the vertex finding algorithm on the results, the analysis was repeated using a different algorithm. This second algorithm differs from the standard algorithm used in that it makes separate requirements on the $|d_0|$ of the higher and lower momentum tracks (>1 mm and >3 mm respectively), rejects vertex candidates with $\alpha > 2°$, makes a much looser cut on the separation in z of the two tracks at the vertex (80 cm as opposed to 20 cm for the standard algorithm), and does not make any requirements on the variable X. In the case of two vertices passing the requirements the one at smaller radius is chosen. This second vertex finder provides a cleaner sample of K^0_S's, however, it is less efficient than the standard vertex finder by a factor of ∼1.6. The difference in the inclusive K^0_S branching ratios measured using the two vertex finders was negligible, and therefore no systematic error was assigned due to the vertex finding algorithm.

The vertex finding efficiency is also affected by how well the Monte Carlo models various detector effects. Two effects which deserve special attention are track finding inefficiencies near the anode and cathode planes in the jet-chamber, and the two-track resolution of the jet-chamber which leads to a reduced efficiency for finding K^0_S's with small $\pi^+\pi^-$ opening angles.

The first of these effects was investigated by looking at distributions of the number of vertices found as a function of ϕ in data and Monte Carlo. No significant differences were found, so no

systematic error was assigned because of problems modelling the efficiency of the jet-chamber near the anode and cathode planes.

The potential problem of two-track resolution was examined using distributions of the opening angle of the two tracks making up the vertex. Although no explicit cut was made on this quantity, differences between the efficiencies predicted from Monte Carlo and those actually observed in the data at small opening angles could cause systematic shifts in the measured branching ratios. The minimum opening angles observed in the data and MC, however, lie well above the region where significant efficiency loss due to two track resolution is expected (<5 mrad opening angle). Further, if the analysis is repeated applying cuts on the $\pi^+\pi^-$ opening angle between 15 and 50 mrad, no difference in the branching ratios is found compared to the standard calculation within the statistics of the check. No systematic error was therefore assigned for this effect.

Monte Carlo Statistics

Finite Monte Carlo statistics resulted in uncertainties on the efficiencies and bias factor used in the branching ratio calculations. These statistical uncertainties were included as systematic errors.

Track Related Systematics

Systematic effects from inadequacies of the modelling of track p_t, the number of z-chamber hits per track, and the angle between the V_0 flight direction and momentum, α, were estimated by comparing the ratios of events passing the cuts to the number of vertex candidates, between data and Monte Carlo. The differences in data and MC ratios were used to assign the systematic errors.

Residual Conversions

As photon conversions which remain in the K^0_S and K^* data sets are expected to have a broad $M_V(\pi^+\pi^-)$ mass distribution if the electrons are mistakenly identified as pions, they can fall in the $M_V(\pi^+\pi^-)$ signal region and be mistakenly counted in the branching ratio calculation. The fraction of events in the data with $M_V(e^+e^-) < 0.15$ GeV (assumed to be conversions) is seen to fall linearly with $M_V(\pi^+\pi^-)$. Thus, the expected number of conversions in the K^0_S mass window could be estimated by extrapolating the numbers of events with $M_V(e^+e^-) < 0.15$ GeV in several mass regions outside the K^0_S window, to the K^0_S mass window (0.475–0.520 GeV) using a linear extrapolation function. The systematic error from residual conversions in the final event samples was then estimated to be the difference between the observed fraction of events in the K^0_S signal region failing the $M_V(e^+e^-)$ cut and the expected fraction from the linear extrapolation described above.

Non-tau Background in the Pre-Selection

The error on $f^{non-\tau}_{pre-sel}$ comes from the statistics of the Monte Carlo and data control samples used to estimate the non-tau backgrounds in the $e^+e^- \to \tau^+\tau^-$ pre-selection. These are described in more detail in reference [18].

7 Summary and Discussion

Including the systematic errors given above, our measurements of the inclusive branching ratios of tau leptons to K^0_S and K^{*-} are:

$$\begin{aligned} Br(\tau^- \to K^0_S X^- \nu_\tau) &= 0.86 \pm 0.08(\text{stat.}) \pm 0.05(\text{syst.})\ \% \\ Br(\tau^- \to K^{*-} \geq 0 h^0 \nu_\tau) &= 1.73 \pm 0.24(\text{stat.}) \pm 0.13(\text{syst.})\ \%. \end{aligned}$$

where X^- refers to any configuration of particles with charge -1 and h^0 is any neutral hadron other than K^0_S.

Both the $\tau^- \to K^0_S X^- \nu_\tau$ and the $\tau^- \to K^{*-} \geq 0 h^0 \nu_\tau$ branching ratios are reasonably consistent with, although slightly higher than, the 1992 Particle Data Group world average values of $0.64 \pm 0.15\%$ and $1.43 \pm 0.17\%$, respectively[3] and with the sum of recent exclusive measurements of $\tau^- \to K^0_L h^- \geq 0 h^0 \nu_\tau$ modes by the ALEPH collaboration [8]. The OPAL measurement of $Br(\tau^- \to K^{*-} \geq 0 h^0 \nu_\tau)$, is also consistent with, although slightly higher than, the Particle Data Group world average and the ALEPH result for the exclusive decay $\tau^- \to K^{*-} \nu_\tau$ ($1.42 \pm 0.18\%$ and $1.45 \pm 0.17\%$ respectively), and is very similar to the recent DELPHI result [9] ($1.7 \pm 0.7\%$), indicating that the contribution of states with π^0's to $\tau^- \to K^{*-} \geq 0 h^0 \nu_\tau$ is small. Additionally, $\sim 30\%$ of our $\tau^- \to K^0_S X^- \nu_\tau$ events are observed to originate from sources other than the $K^{*-}(892)$ resonance, in general agreement with phenomenological predictions [4, 5].

8 Acknowledgements

It is a pleasure to thank the SL Division for the efficient operation of the LEP accelerator, the precise information on the absolute energy, and their continuing close cooperation with our experimental group. In addition to the support staff at our own institutions we are pleased to acknowledge the
Department of Energy, USA,
National Science Foundation, USA,
Texas National Research Laboratory Commission, USA,
Particle Physics and Astronomy Research Council, UK,
Natural Sciences and Engineering Research Council, Canada,
Fussefeld Foundation,
Israeli Ministry of Energy and Ministry of Science,
Israel Science Foundation, administered by the Israel Academy of Science and Humanities,
Minerva Gesellschaft,
Japanese Ministry of Education, Science and Culture (the Monbusho) and a grant under the Monbusho International Science Research Program,
German Israeli Bi-national Science Foundation (GIF),
Direction des Sciences de la Matière du Commissariat à l'Energie Atomique, France,
Bundesministerium für Forschung und Technologie, Germany,
National Research Council of Canada,
A.P. Sloan Foundation and Junta Nacional de Investigação Científica e Tecnológica, Portugal.

References

[1] T.Das, V.S.Mathur, S.Okubo, Phys. Rev. Lett. **18** (1967) 761.

[2] S.Oneda, Phys. Rev. **D35** (1987) 397.

[3] Particle Data Group, Phys. Rev. **D45** (1992).

[4] see for example,
B.C.Barish, R.Stroynowski, Phys. Rep. **157** (1988) 1,
F.Gilman, S.Rhie, Phys. Rev. **D31** (1985) 1066.

[5] S.Jadach, Z.Wąs, R.Decker, J.H.Kühn, Comput. Phys. Commun. **76** (1993) 361; TAUOLA Version 2.4.
S.Jadach, Z.Wąs, R.Decker, J.H.Kühn, Comput. Phys. Commun. **64** (1991) 275; TAUOLA Version 1.5.

[6] DELCO Collaboration, G.B.Mills, *et al.*, Phys. Rev. Lett. **54** (1985) 624.

[7] H.J.Lipkin, Phys. Lett. **B303** (1993) 119.
E.L.Berger, H.J.Lipkin, Phys. Lett. **B189** (1987) 226.

[8] ALEPH Collaboration, D.Buskulic, *et al.*, CERN PPE/94-59 (submitted to Phys. Lett. B).
ALEPH Collaboration, D.Buskulic, *et al.*, CERN PPE/94-58 (submitted to Phys. Lett. B).

[9] DELPHI Collaboration, P.Abreu, *et al.*, CERN PPE/94-88 (submitted to Phys. Lett. B).

[10] CLEO Collaboration, M.Goldberg, *et al.*, Phys. Lett. **B251** (1990) 223.

[11] ARGUS Collaboration, H.Albrecht, *et al.*, Z. Phys. **C41** (1988) 1.

[12] HRS Collaboration, R.Tschirhart, *et al.*, Phys. Lett. **B205** (1988) 223.

[13] TPC/2γ Collaboration, H.Aihara, *et al.*, Phys. Rev. Lett. **59** (1987) 751.

[14] TPC/2γ Collaboration, H.Aihara, *et al.*, Phys. Rev. **D35** (1987) 1553.

[15] Mark II Collaboration, J.M.Yelton, *et al.*, Phys. Rev. Lett. **56** (1986) 812.

[16] OPAL Collaboration, K.Ahmet, *et al.*, Nucl. Instr. and Meth. **A313** (1992) 103.

[17] P.P.Allport, *et al.*, Nucl. Instr. and Meth. **A324** (1993) 34.

[18] OPAL Collaboration, P.Acton, *et al.*, Phys. Lett. **B328** (1994) 207.
OPAL Collaboration, G.Alexander, *et al.*, Phys. Lett. **B266** (1991) 201.
OPAL Collaboration, G.Alexander, *et al.*, Z. Phys. **C52** (1991) 175.

[19] S.Jadach, B.F.L.Ward, Z.Wąs, Comput. Phys. Commun. **79** (1994) 503; KORALZ Version 4.0.
S.Jadach, B.F.L.Ward, Z.Wąs, Comput. Phys. Commun. **66** (1991) 276; KORALZ Version 3.8.

[20] J.Allison, *et al.*, Nucl. Instr. and Meth. **A317** (1992) 47.

[21] OPAL Collaboration, P.Acton, *et al.*, Phys. Lett. **B305** (1993) 407.

[22] U.Maur, Dissertation, University of Bonn, **BONN-IR-94-06** (1994).

Figure Captions

Figure 1:
Distributions of several variables used in the inclusive K^0_S and K^* samples, with all cuts applied except the one on the variable being plotted. Plot a) shows the radial distance of the secondary vertex from the primary vertex. Note that events rejected by the cut requiring the radius of the vertex to be greater than 1 cm are not included in this plot. Plot b) is of the angle, α, between the V_0 momentum and flight path vectors. Plot c) gives the invariant mass distribution of the two tracks making up the vertex assuming that they are electrons. Plot d) shows the number of good tracks, besides the two vertex tracks, in the same hemisphere as the vertex momentum vector. In all of the plots the points correspond to 1990–1992 data, the hatched histogram is the background predicted from events outside of the $M_V(\pi^+\pi^-)$ mass peak scaled to the background fitted under the peak, and the open histogram is the sum of the background and the $\tau\to K^*\to K^0_S$ MC sample. Arrows on the plots indicate the cut values applied in the analysis.

Figure 2:
The $\pi^+\pi^-$ invariant mass distribution of the vertex tracks in the inclusive K^0_S data sample showing the 1990–1992 data (points), the Gaussian plus linear background fit to the data used for systematic studies (dashed line), and the prediction of the τ-decay MC (solid histogram). Also shown are the peak and sideband regions used for signal and background estimation.

Figure 3:
The K^0_S-h^- invariant mass distribution in the $K^0_S h^- \geq 0 h^0$ data sample, when constraining $M_V(\pi^+\pi^-)$ to equal $M_{K^0_S}$, and when assuming a pion mass for the h^-. The points represent the 1990–1992 data, the solid line is the spin-1 Breit-Wigner resonance plus second order polynomial fit to the data, the single-hatched area is the contribution of the second order polynomial to the fit, and the double-hatched histogram is the non-K^0_S background predicted from events in the region of the $M_V(\pi^+\pi^-)$ plot outside of the signal region. Also shown are the peak and sideband regions used for signal and background estimation in the systematic studies.

Figure 4:
The efficiency of the inclusive K^0_S selection (not including the $K^0_S\to\pi^+\pi^-$ branching ratio) with respect to the pre-selected events predicted by the $\tau\to K^*\to K^0_S$ MC, as a function of, a), the K^0_S polar angle, and b), the K^0_S momentum. Also shown are the reconstructed K^0_S-candidate, and K^*-candidate momenta — plots c) and d) respectively. The points are the 1990–1992 data, the hatched histogram is the background predicted from data events outside of the $M_V(\pi^+\pi^-)$ signal region, and the open histogram is the sum of this background and the prediction from $\tau\to K^*\to K^0_S$ MC events.

Figure 5:
The $\sum|d_0|$ distribution in the inclusive K^0_S sample without the $\sum|d_0|$ cut applied in the vertex finder. The points are the 1990–1992 data, the hatched histogram is the background predicted from data events outside of the $M_V(\pi^+\pi^-)$ signal region, and the open histogram is the sum of this background and the prediction from $\tau\to K^0_S\to\pi^+\pi^-$ MC events.

Figure 1

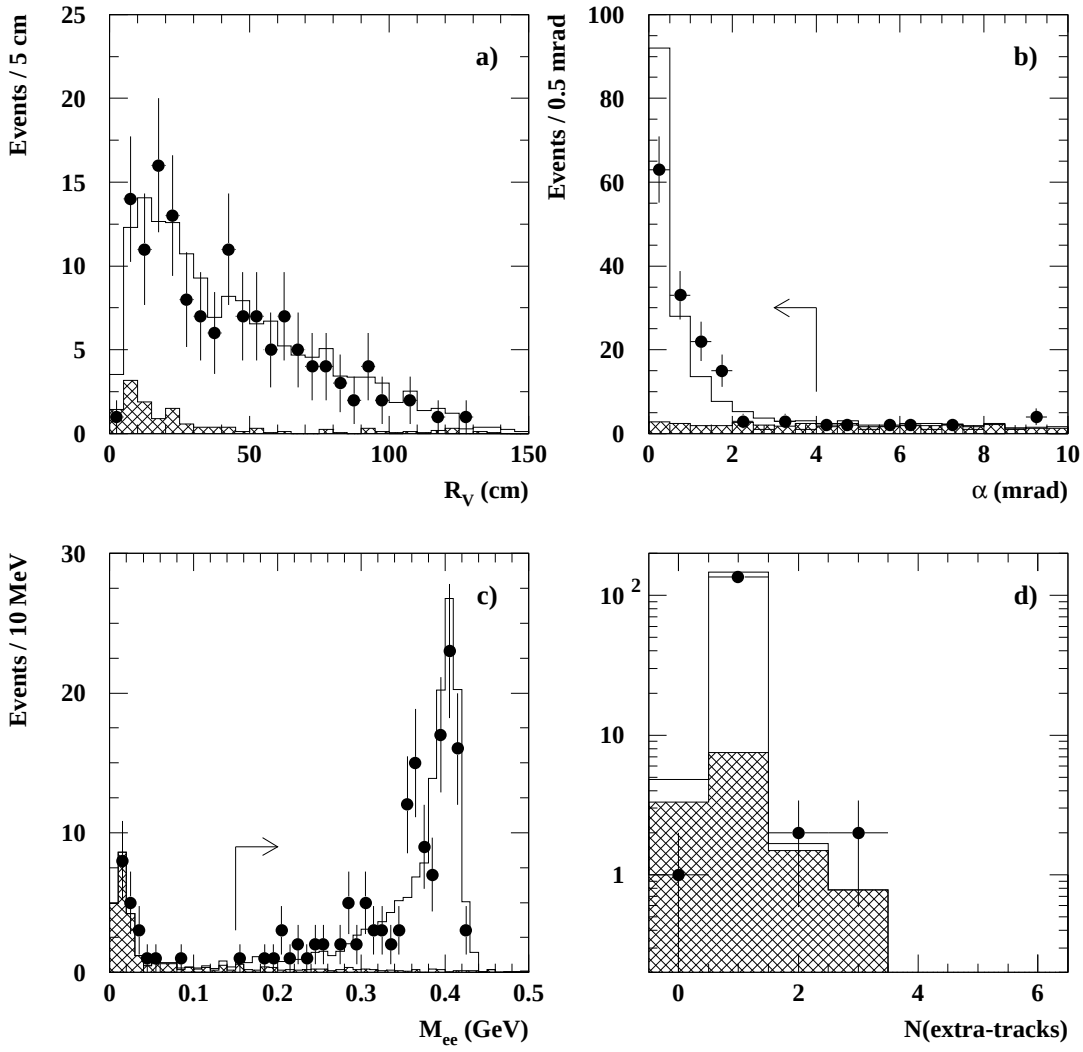
Events / 5 cm
a)
R_V (cm)
Events / 0.5 mrad
b)
α (mrad)
Events / 10 MeV
c)
M_{ee} (GeV)
d)
N(extra-tracks)

Figure 2

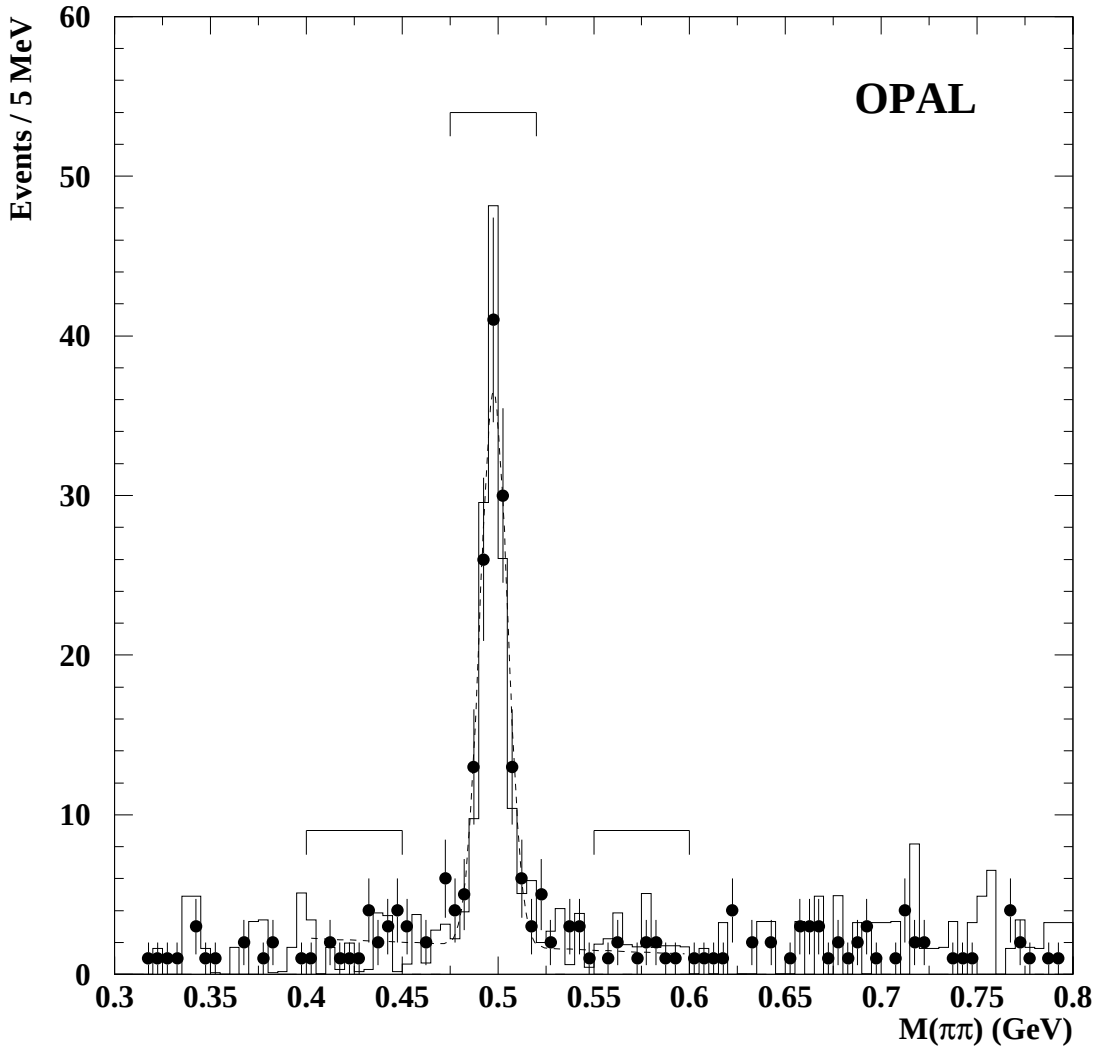
OPAL
Events / 5 MeV
60
50
40
30
20
10
0
0.3
0.35
0.4
0.45
0.5
0.55
0.6
0.65
0.7
0.75
0.8
M(ππ) (GeV)

Figure 3

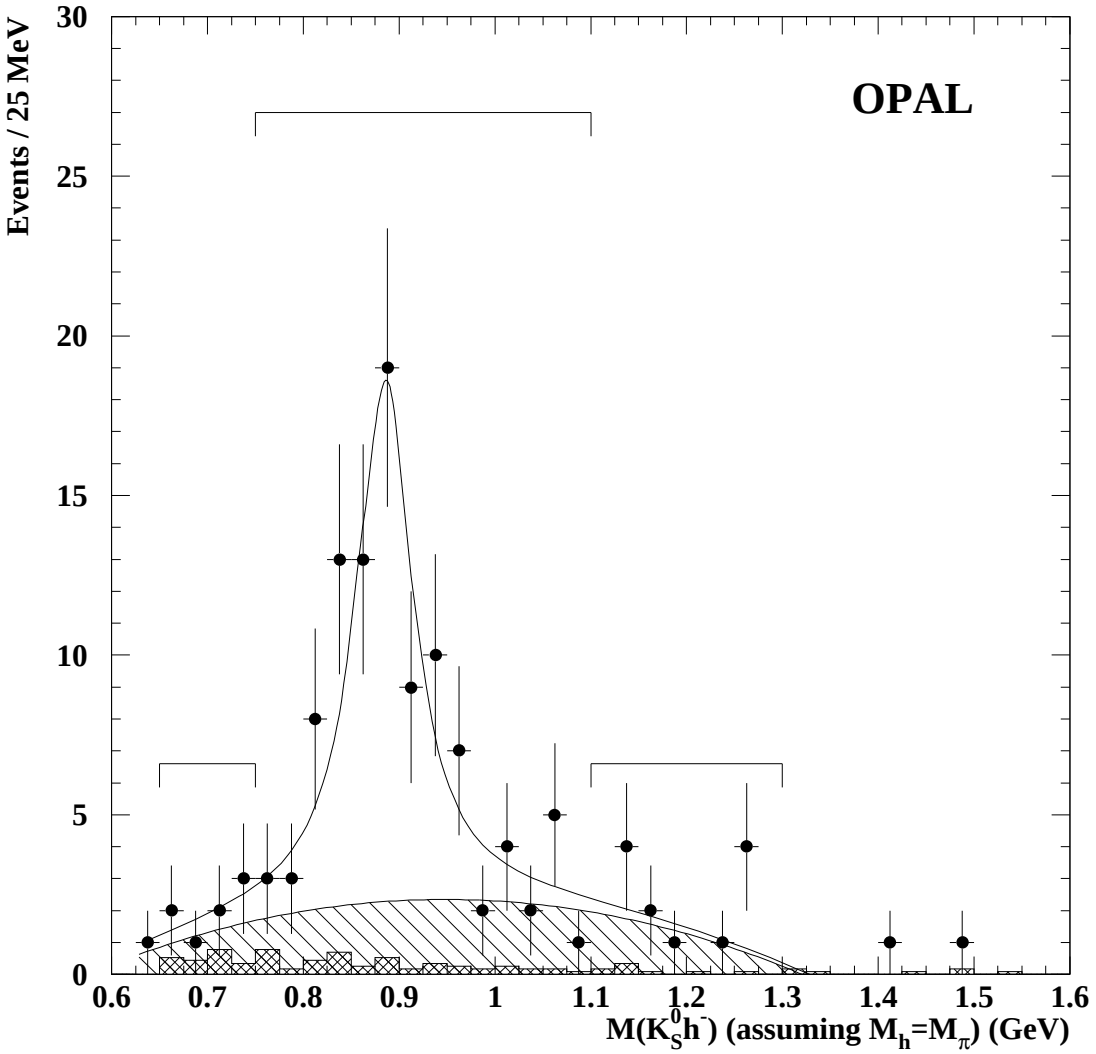
OPAL
Events / 25 MeV
30
25
20
15
10
5
0
0.6
0.7
0.8
0.9
1
1.1
1.2
1.3
1.4
1.5
1.6
M(K^0_Sh$^-$) (assuming M$_h$=M$_\pi$) (GeV)

Figure 4

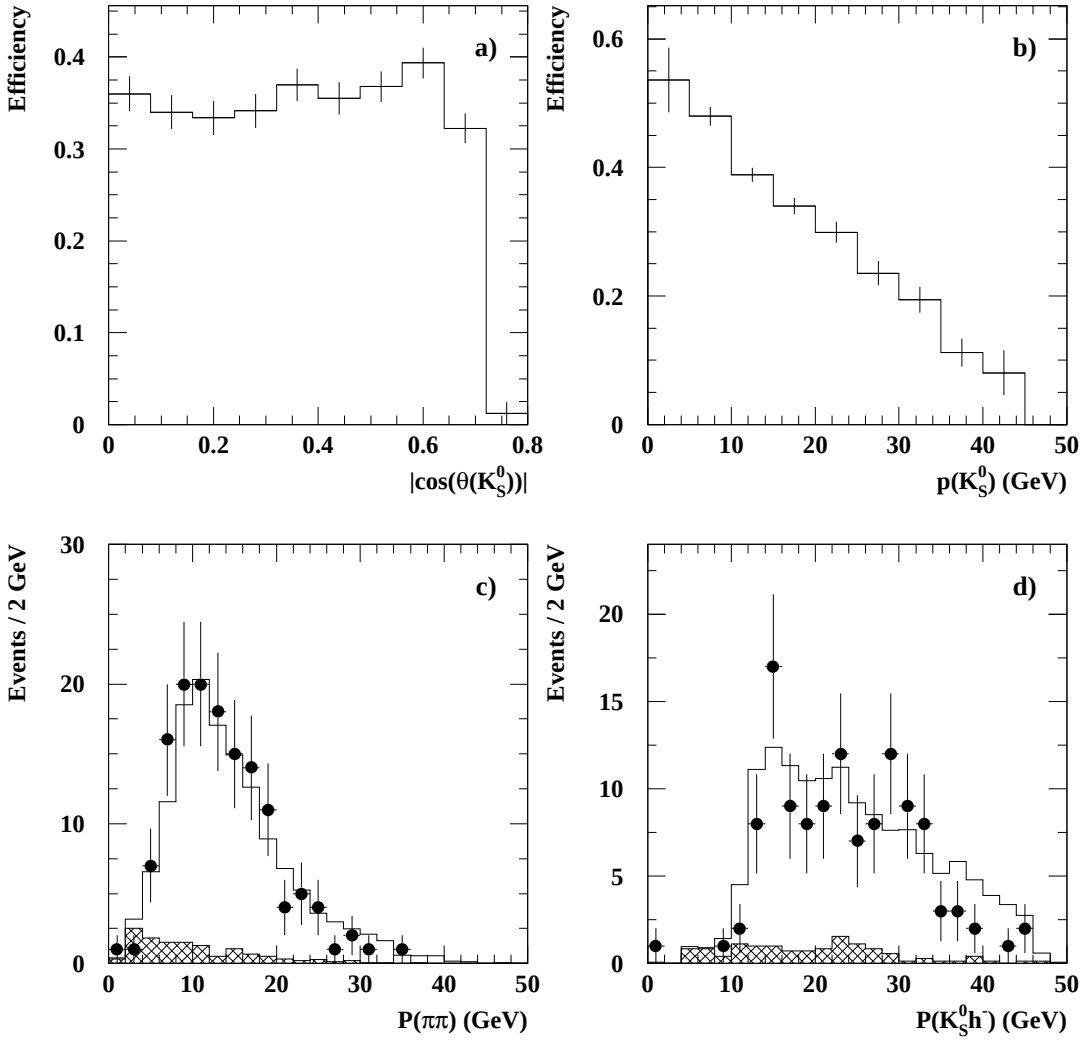
Efficiency
a)
$|\cos(\theta(K^0_S))|$
Efficiency
b)
$p(K^0_S)$ (GeV)
Events / 2 GeV
c)
$P(\pi\pi)$ (GeV)
Events / 2 GeV
d)
$P(K^0_S h^-)$ (GeV)

Figure 5